Probing Molecular Structures of Poly (dimethyl siloxane) at Buried Interfaces in Situ

ARTICLE *in* THE JOURNAL OF PHYSICAL CHEMISTRY C · FEBRUARY 2013

Impact Factor: 4.77

1 AUTHOR:

Chi Zhang

Purdue University

33 PUBLICATIONS **222** CITATIONS

SEE PROFILE

THE JOURNAL OF PHYSICAL CHEMISTRY C

Article

pubs.acs.org/JPCC

Probing Molecular Structures of Poly(dimethylsiloxane) at Buried Interfaces *in Situ*

Chi Zhang and Zhan Chen*

Department of Chemistry, University of Michigan, 930 North University Avenue, Ann Arbor, Michigan 48109, United States

Supporting Information

ABSTRACT: Silicone materials such as poly(dimethylsiloxane) (PDMS) are widely used in a variety of important applications such as polymer adhesives, packaging materials for microelectronics, polymer MEMS, microfluidics, biomedical implants, and marine antifouling coatings. In such applications, molecular structures of PDMS at buried interfaces will determine interfacial properties. Therefore, it is important to elucidate PDMS molecular structures at relevant buried interfaces. In this study, the interfacial structures of PDMS silicone elastomer in contact with silica and different polymer materials have been studied using sum frequency generation (SFG) vibrational spectroscopy. It was found that the PDMS methyl groups are ordered at the buried poly(ethylene terephthalate) (PET)/PDMS and fused silica/PDMS interfaces. However, these methyl groups tend to adopt different orientations at different interfaces. Using the SFG spectral fitting results, the possible ranges of tilt angles and twist angles of PDMS methyl groups at the buried PET/PDMS and silica/PDMS interfaces were determined. At the PET/PDMS interface, the methyl groups tend to have large tilt angles (>70°) with small twist angles (<20°). At the silica/PDMS interface, methyl groups tend to adopt a broad distribution of tilt angles along with large twist angles. The absolute orientations of the PDMS methyl groups at the buried interfaces were determined from the interference pattern of the PDMS SFG signal with the nonresonant signal from a TiO_2 thin film. PDMS methyl groups tend to orient toward the PDMS bulk rather than the contacting substrates at both the PET/PDMS and silica/PDMS interfaces. However, at the polystyrene/PDMS and poly(methyl methacrylate)/PDMS interfaces, PDMS methyl groups orient toward the hydrophobic polymer substrate surfaces. The different orientations of PDMS methyl groups at the investigated buried interfaces were correlated to interfacial polar interactions determined by substrate surface hydrophobicities.

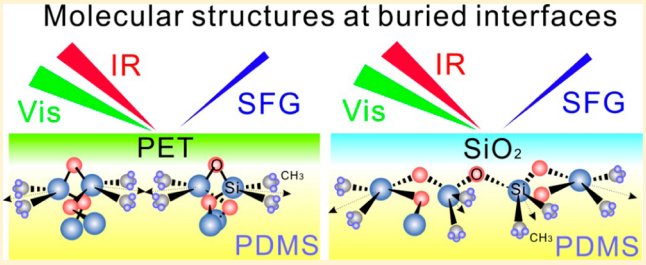

1. INTRODUCTION

Silicone elastomers such as poly(dimethylsiloxane) (PDMS) are extensively used in many important applications such as polymer adhesives, packaging materials for microelectronics, polymer MEMS, microfluidics, biomedical implants, and marine antifouling coatings. For example, polymer adhesives based on silicone materials including PDMS have played a key role in the development of electronic devices used in solar, LED, computer and automotive applications, and durable structures used in green housing, office buildings, bridges, and roads. PDMS materials have such a wide variety of applications due to their high thermal stability, excellent rheological properties, low temperature flexibility, UV resistance, and simple, controllable cure chemistry.[1,2] They are sustainable because in principle they can be prepared from sand and carbon, which are inexhaustible on earth.

Molecular structures of PDMS at buried interfaces primarily determine interfacial properties. For example, adhesion properties of silicone elastomers are believed to be related to the molecular interfacial structures of PDMS, such as coverage or orientation of interfacial functional groups. Sometimes, adhesion promoters such as organosilanes are used to improve adhesion because pure silicone elastomers tend to have weak adhesion to certain substrates including polymers.[3−5] In order to understand the adhesion of PDMS materials with or without silane adhesion promoters added, it is important to study molecular interfacial structures of PDMS at different polymer interfaces.

Many surface-sensitive techniques have been used to study molecular structures on polymer surfaces or at polymer interfaces.[6−9] Currently it is still quite challenging to study molecular structures at buried interfaces *in situ*. Recently, sum frequency generation (SFG) vibrational spectroscopy has been developed into a powerful tool to study molecular structures at buried interfaces.[10−28] SFG can probe vibrational modes of various functional groups at interfaces, providing molecular insight into interfacial structures of complicated molecules. Furthermore, by collecting SFG spectra with different input and output beam polarization combinations, the molecular orientation of certain functional groups can be derived.[29−33]

Surface and interfacial structures of PDMS have been studied using SFG by several groups. The first SFG study on PDMS

Received: July 27, 2012
Revised: January 31, 2013
Published: February 1, 2013

was published in 1997 by Zhang et al.[34] It was reported that the surface of a polyurethane material terminated with PDMS end groups restructured in water. In 2004, Chen et al. investigated the polymer/air and polymer/water interfaces of several model PDMS materials.[35] The results suggested that all the PDMS surfaces studied were mainly covered by methyl groups. Surface restructuring of the methyl groups has also been observed in water. Yurdumakan et al. used SFG to study the buried PDMS/polystyrene (PS) interface to elucidate the friction property at the interface.[36] They also studied the buried interfaces between oxidized PDMS or regular PDMS and SAMs. It was concluded that the enhanced ordering of PDMS can be induced by both the confinement at the interface and the template of the SAM methyl groups.[37] Ye et al. applied SFG to study PDMS surface changes after various treatments, such as plasma and UV irradiation.[38] The chain conformation of a PDMS monolayer at the air/water interface has also been studied using SFG.[39] It was found that methyl groups of PDMS chains at the interface are disordered in the dilute regime, while two methyl groups on the repeating unit point to air asymmetrically with higher PDMS surface densities. Ye et al. studied surface structures of PDMS materials incorporated with biocides and other functionalities for marine antifouling and fouling-release coating applications. Surface restructuring behaviors of various PDMS materials have been followed in detail using SFG.[40−42] SFG has also been applied to study molecular interactions at buried polymer/silane interfaces[15,43−45] and various polymer/PDMS (with or without silane adhesion promoters) interfaces.[27,28,46,47]

We have previously shown that polymer materials can exhibit varied structures when in contact with different media.[25] For example, poly(ethylene glycol) can have different interfacial structures when in contact with different polymers.[48] In this study, we investigated interfacial structures of PDMS in contact with poly(ethylene terephthalate) (PET) and fused silica. SFG studies showed that PDMS methyl groups adopt different orientations at these two different interfaces. Methyl group orientations at different interfaces before and after curing were also compared. We further validated our spectral fitting results according to the interference between the PDMS SFG signal and the nonresonant SFG signal from a TiO_2 thin film. Moreover, absolute orientations of interfacial methyl groups of PDMS at these two interfaces as well as other two interfaces between PDMS and hydrophobic polymers were determined, which was correlated to the hydrophobic properties of the contacting substrates.

2. EXPERIMENTAL SECTION

2.1. Sum Frequency Generation (SFG) Vibrational Spectroscopy. SFG is a second order nonlinear optical process which probes the second-order nonlinear optical susceptibility of the sample. Selection rule provides SFG submonolayer surface and interface sensitivity. Under the electric dipole approximation, no SFG signal can be generated from a centrosymmetric bulk medium. SFG signal can only be generated at surfaces or interfaces where the centrosymmetry is broken. The theory of SFG and the details of our SFG spectrometer have been reported in previous publications.[11−13,29,30,32,49−54] In this study, the visible and mid-infrared (IR) input beams penetrated through a fused silica substrate and overlapped at the interface spatially and temporally. The beam diameters at the sample interface were about 400 μm. The pulse energies of the visible and IR beams were ~30 and ~100 μJ, respectively. The input angles of visible and IR beams were 60° and 57° vs the surface normal, respectively. The SFG signal was collected by a monochromator along with a photomultiplier tube (PMT). SFG spectra in the experiment were collected using ssp (s-polarized sum frequency output, s-polarized visible input, and p-polarized IR input) and sps polarization combinations with the near critical angle geometry (Figure 1).[27] The large refractive angle at the interface provides stronger reflection SFG signals compared to those from the regular reflection geometry.[27,55]

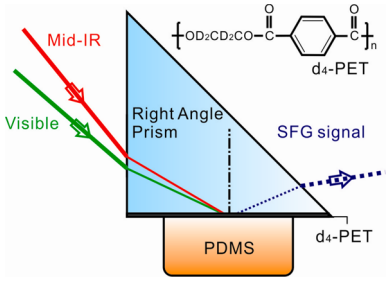

Figure 1. The near total reflection geometry used in the experiment for interface studies. To clearly show the SFG reflection signal, the reflected mid-IR and visible beams were not plotted. The molecular formula of d_4-PET is displayed on the top right.

2.2. Sample Preparation. In order to avoid spectral confusion, PET samples with aliphatic chain deuterated (d_4-PET) were used in the experiment, which was obtained from Polymer Source Inc. The d_4-PET was dissolved in 2-chlorophenol (Sigma-Aldrich) to form a 1 wt % solution. The polymer thin films were then prepared by spin-coating the 1 wt % polymer solution on fused silica prisms at 2500 rpm. d_8-PS and d_8-poly(methyl methacrylate) (d_8-PMMA) were also obtained from Polymer Source Inc. The procedure of making d_8-PS and d_8-PMMA samples were similar to that of d_4-PET thin film. The PDMS samples were prepared by using Sylgard 184 silicone elastomer kit, which was obtained from Dow Corning Corporation. The Sylgard 184 silicone elastomer was mixed in 10:1 base/curing agent ratio using a vortex mixer. For cured interfaces, the samples were cured in the oven at 140 °C for 2 h and then stored at room temperature for 24 h before use. Right angle silica prisms were purchased from Altos Photonics, Inc. They were placed in a concentrated sulfuric acid and potassium dichromate mixture overnight at 60 °C to eliminate hydrocarbon contaminations. Then they were rinsed with deionized water and further cleaned in a home-built air plasma cleaner.

TiO_2 thin films used in the experiment were deposited on silica prisms. Before deposition, silica prisms were cleaned using the procedure previously mentioned. The deposition of a Ti thin film was carried out using electron beam physical vapor deposition (EnerJet Evaporator). The environment was oil-free, and the pressure was lower than 2×10^{-6} Torr. The thickness of the deposited Ti film was ~50 nm and was monitored by a quartz crystal oscillator. The substrate was heated at 700 °C for 4 h to form a translucent layer of TiO_2 on fused silica.

In order to compare the interference of the TiO_2 nonresonant SFG signal with the SFG signal from the silica/PDMS interface to the interference of the TiO_2 nonresonant SFG signal with the SFG signal from the polymer/PDMS interface, some fused silica prisms with TiO_2 coating were selected and a thin layer (~50 nm) of silica was coated on the

dx.doi.org/10.1021/jp307472j | J. Phys. Chem. C 2013, 117, 3903−3914

TiO_2 surface of each substrate. The procedure of coating silica on TiO_2 was similar to that of coating Ti on silica.

3. SFG DATA ANALYSIS METHOD

The SFG signal intensity in our experiment can be expressed as

$$I_{SFG} \propto |\chi_{eff}^{(2)}|^2 I_{IR} I_{vis} \quad (1)$$

Here I_{IR} and I_{vis} are intensities of the input IR and visible beams, respectively. $\chi_{eff}^{(2)}$ is the effective second-order nonlinear optical susceptibility which can be expressed as

$$\chi_{eff}^{(2)} = \chi_{NR}^{(2)} + \sum_q \frac{A_q}{\omega_{IR} - \omega_q + i\Gamma_q} \quad (2)$$

$\chi_{NR}^{(2)}$ is the nonresonant contribution from the sample. The resonant contribution can be modeled as the sum of Lorentzians with signal strength or amplitude A_q, frequency ω_q, and line width Γ_q.

For an isotropic surface or interface in the $x-y$ plane, the effective susceptibility components can be correlated to the susceptibility components of the sample defined in lab-fixed coordinates:

$$\chi_{eff,ssp} = L_{yy}(\omega_{SF}) L_{yy}(\omega_{vis}) L_{zz}(\omega_{IR}) \sin\theta_{i,IR} \chi_{yyz} \quad (3)$$

$$\chi_{eff,sps} = L_{yy}(\omega_{SF}) L_{zz}(\omega_{vis}) L_{yy}(\omega_{IR}) \sin\theta_{i,vis} \chi_{yzy} \quad (4)$$

Here, $\theta_{i,IR}$ and $\theta_{i,vis}$ are incident angles of the input IR and visible beams. L_{ii} $(i = x, y, z)$ are Fresnel coefficients which are functions of the laser beam input angles and refractive indices of materials forming the interface.[12]

The measured SFG second-order nonlinear optical susceptibility components can be related to molecular hyperpolarizability components through molecular orientations. Such relations for functional groups with C_{3v} symmetry such as methyl groups have been developed.[30] In PDMS, even though the angles between various chemical bonds can be flexible,[56] the two neighboring methyl groups on average have a fixed bond angle of 112° (as shown in Figure 2). Therefore, the vibrational

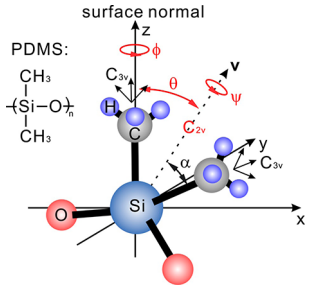

Figure 2. Molecular structure of PDMS and the coordinate system chosen for orientation analysis. Each methyl group presents a C_{3v} symmetry. The entire $Si(CH_3)_2$ group presents a C_{2v} symmetry. The xyz coordinate demonstrates the lab frame. θ, ψ, and ϕ are tilt angle, twist angle, and azimuthal angle of vector **v** that bisects the $Si(CH_3)_2$ group. The molecular formula of PDMS is displayed on the left.

mode hyperpolarizabilities of the two individual methyl groups need to be combined in the molecular frame. For a $Si(CH_3)_2$ group, the transformation between lab frame and molecular frame can be achieved using a united atom model for each methyl group.[57] The two methyl groups connected to the same Si atom are then considered to adopt a C_{2v} symmetry, while each methyl group still has a C_{3v} symmetry. A vector **v**, which bisects the two methyl groups, is used to describe the molecular orientation of these two methyl groups. The angle between the principal axis of each methyl group and the vector **v** is defined as angle α ($\alpha = 56°$). The tilt angle and twist angle which will be discussed in the paper are in reference to this vector **v**. After two coordinate transformations, the second-order nonlinear optical susceptibility components of the $Si(CH_3)_2$ group in PDMS can be expressed as eqs 5–8.[57]

Symmetric stretch:

$$\chi_{yyz} = \chi_{xxz} = (N/2\varepsilon_0)(\beta_{aac} - \beta_{ccc})\{(\cos\theta - \cos^3\theta)[(5 + 3\cos 2\psi)(\cos\alpha - \cos^3\alpha) - 2\cos\alpha] - 2\cos\theta(\cos\alpha - \cos^3\alpha)\} + (2N/\varepsilon_0)\beta_{aac}\cos\theta\cos\alpha \quad (5)$$

$$\chi_{yzy} = \chi_{zxx} = \chi_{xzx} = (N/2\varepsilon_0)(\beta_{aac} - \beta_{ccc})[(\cos\theta - \cos^3\theta)(5 + 3\cos 2\psi)(\cos\alpha - \cos^3\alpha) + 2\cos\theta\cos\alpha(\cos^2\theta + \cos^2\alpha - 2)] \quad (6)$$

Asymmetric stretch:

$$\chi_{yyz} = \chi_{xxz} = (N/\varepsilon_0)\beta_{caa}\{[-2\cos\theta + 3(\cos\theta - \cos^3\theta)(1 + \cos 2\psi)](\cos\alpha - \cos^3\alpha) - 2(\cos\theta - \cos^3\theta)\cos^3\alpha\} \quad (7)$$

$$\chi_{yzy} = \chi_{zxx} = \chi_{xzx} = (N/\varepsilon_0)\beta_{caa}[3(\cos\theta - \cos^3\theta)(\cos\alpha - \cos^3\alpha)(1 + \cos 2\psi) + 2\cos^3\theta\cos^3\alpha] \quad (8)$$

Here, N is the surface number density of detected functional groups, ε_0 is the permittivity of free space. β_{aac}, β_{ccc}, and β_{caa} are the hyperpolarizability components of the single methyl group C–H stretching modes. χ_{yyz}, χ_{xxz}, χ_{yzy}, χ_{zxx}, and χ_{xzx} are second-order nonlinear optical susceptibility components of the C–H stretching modes for $Si(CH_3)_2$ defined in the lab-fixed coordination system. Furthermore, it is assumed in eqs 5–8 that the sample is isotropic in the $x-y$ plane, and therefore the azimuthal angle ϕ can be averaged. The angle θ is the tilt angle of vector **v** of the entire $Si(CH_3)_2$ group (vs the surface normal), and ψ is the twist angle of the same group.

The values of β_{aac}, β_{ccc}, and β_{caa} can be obtained by calculation. It has been reported that the ratio of β_{aac}/β_{ccc} is in the range of 1.6–4.3 for a methyl group.[12] For a PDMS methyl group, the ratio $\beta_{aac}/\beta_{ccc} = 2.3$ has been applied in previous publications[58,59] based on the bond additivity method. $\beta_{aac}/\beta_{caa} \approx 1$ has also been reported for a methyl group.[30] In this research, we first provide numerical analysis based on eqs 5–8 by assigning values $\beta_{aac}:\beta_{ccc}:\beta_{caa} = 2.3:1:2.3$ and $\beta_{ccc} = 1$. Calculated values of $\chi_{yyz,s}\varepsilon_0/N$, $\chi_{yyz,as}\varepsilon_0/N$, and the ratios of $\chi_{yyz,s}/\chi_{yyz,as}$ and $\chi_{yyz,as}/\chi_{yzy,as}$ were plotted as functions of tilt angle θ and twist angle ψ (Figure 3). Taken eqs 3 and 4 into consideration, it is possible to deduce the possible range of the molecular orientation of the methyl groups in PDMS based on the SFG symmetric and asymmetric stretching signals detected using ssp and sps polarization combinations. Either the ratio of $\chi_{yyz,s}/\chi_{yyz,as}$ or $\chi_{yyz,as}/\chi_{yzy,as}$ obtained from the experiment is possible to be used to define a range of angle θ and ψ. In this research, we deduced both ratios and compared the possible orientation angle ranges assuming a δ-orientation angle distribution. Although interfacial methyl groups may not

dx.doi.org/10.1021/jp307472j | J. Phys. Chem. C 2013, 117, 3903–3914

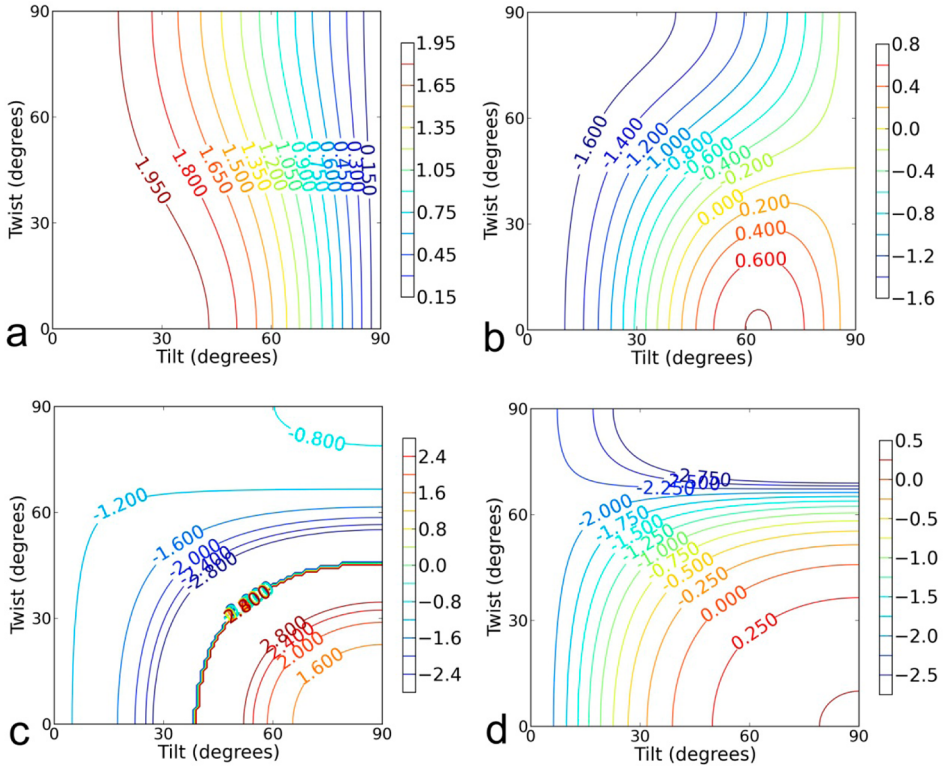

Figure 3. Calculated values of (a) $\chi_{yyz,s}\varepsilon_0/N$ and (b) $\chi_{yyz,as}\varepsilon_0/N$ and ratios of (c) $\chi_{yyz,s}/\chi_{yyz,as}$ and (d) $\chi_{yyz,as}/\chi_{yzy,as}$ are plotted as functions of tilt angle θ and twist angle ψ, with the angle ranges between 0° and 90°. It was assumed that β_{aac}:β_{ccc}:β_{caa} = 2.3:1:2.3 and β_{ccc} = 1 based on the previous publications.

adopt a δ-orientation distribution, the δ-distribution orientation angle deduced here can be considered to represent the average orientation of the methyl groups. The overlapping orientation angle region obtained by these two ratios was considered to be the likely molecular orientations that PDMS methyl groups tended to adopt. From Figures 3c and 3d, we find that the value of $\chi_{yyz,s}/\chi_{yyz,as}$ can be positive or negative due to different tilt angle and twist angle combinations. Positive values tend to hold at the right bottom corner, when tilt angle is big (>40°) and twist angle is small (<50°). On the other hand, when tilt angle is small (<40°) or twist angle is big (>50°), $\chi_{yyz,s}/\chi_{yyz,as}$ will have negative values. For the values of $\chi_{yyz,as}/\chi_{yzy,as}$, this trend is similar.

4. RESULTS AND DISCUSSION

In this paper, SFG has been applied to study interfacial molecular structures of PDMS while in contact with d_4-PET and silica. The ssp SFG spectra collected from d_4-PET/PDMS interfaces are shown in Figures 4a and 4b. Using eq 2, both spectra can be fitted to get the amplitude A_q, frequency ω_q, and line width Γ_q of the vibrational modes. The spectral fitting results are listed in Table 1. All the SFG ssp spectra between 2800 and 3000 cm^{-1} in the aliphatic C−H stretching frequency range were dominated by two peaks. One peak was centered at 2900 cm^{-1}, contributed by the symmetric C−H stretching mode of the Si−CH_3 group. The second peak was centered around 2962 cm^{-1}, generated by the asymmetric C−H stretching mode of the same group. These two strong signals in the SFG spectra indicate that PDMS methyl groups are ordered at the buried d_4-PET/PDMS interfaces, regardless of curing or not. The PDMS methyl symmetric C−H stretching peak center was slightly red-shifted from that detected at the

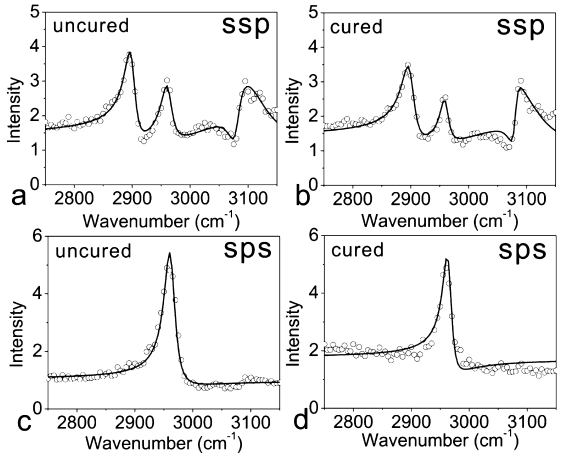

Figure 4. (a, c) The ssp/sps SFG spectra collected from the d_4-PET/PDMS interface before curing and (b, d) after curing. Dots are measured data; lines are fitting results.

air/PDMS interface[39] as well as that of the silica/PDMS interfaces which will be discussed below. Such a shift may be due to the interactions between PDMS methyl groups and the carbon oxygen double bonds in the PET substrate at the interface. At these d_4-PET/PDMS interfaces, in addition to the PDMS methyl signals, SFG signals at around 3100 cm^{-1} were also observed, showing that the d_4-PET aromatic group was also ordered at the interfaces. However, we are not able to quantify the molecular orientation of the d_4-PET aromatic ring because its vibrational signals from various modes cannot be clearly distinguished.

dx.doi.org/10.1021/jp307472j | J. Phys. Chem. C 2013, 117, 3903−3914

Table 1. Spectral Fitting Results for the SFG Spectra Shown in Figure 4

interfaces	ω_q (cm^{-1})	A_q	Γ_q (cm^{-1})	$\lvert A_q/\Gamma_q \rvert$	assignment
d_4-PET/PDMS (uncured, ssp)	2900	13.7 ± 0.9	11.2 ± 0.8	1.22 ± 0.12	Si−CH_3(s)
	2962	11.3 ± 0.7	11.5 ± 0.8	0.98 ± 0.09	Si−CH_3(as)
d_4-PET/PDMS (cured, ssp)	2900	15.6 ± 1.0	13.4 ± 0.6	1.16 ± 0.09	Si−CH_3(s)
	2960	7.7 ± 0.5	9.0 ± 0.5	0.86 ± 0.07	Si−CH_3(as)
d_4-PET/PDMS (uncured, sps)	2962	23.8 ± 0.9	11.5 ± 0.8	2.07 ± 0.16	Si−CH_3(as)
d_4-PET/PDMS (cured, sps)	2965	16.4 ± 0.8	9.0 ± 0.6	1.82 ± 0.15	Si−CH_3(as)

Comparing the SFG spectra collected from the d_4-PET/PDMS interfaces before and after curing PDMS, it was found that the SFG spectral features of the PDMS methyl symmetric and asymmetric C−H stretching modes were similar, even though the intensities of the two peaks for PDMS before and after curing were slightly different. The fitted ratios of $\chi_{ssp,s}/\chi_{ssp,as}$ of PDMS methyl groups before and after curing were 1.24 ± 0.17 and 1.35 ± 0.15 (derived from Table 1), indicating that the PDMS methyl groups have a minor difference in orientation at the d_4-PET/uncured PDMS and d_4-PET/cured PDMS interfaces.

The SFG spectra presented in Figure 4 could not be fit using opposite signs for the symmetric and asymmetric C−H stretches, different from fitting the normal methyl symmetric and asymmetric stretching peaks.[57] Therefore, the two peaks were fit using the same sign, which suggested that the two peaks have the same phase. For the SFG signals detected using the same polarization combination, we have $\chi_{ssp,s}/\chi_{ssp,as} = \chi_{yyz,s}/\chi_{yyz,as}$. Therefore, the ratios of $\chi_{yyz,s}/\chi_{yyz,as}$ at the d_4-PET/PDMS interface before and after curing were 1.24 ± 0.17 and 1.35 ± 0.15, respectively.

SFG spectra were also collected in the sps polarization combination from the d_4-PET/PDMS interfaces before and after curing PDMS (Figures 4c and 4d). In sps spectra, only asymmetric C−H stretch at around 2960 cm^{-1} was clearly resolved. From eq 4, such an sps SFG signal corresponds to the nonlinear optical susceptibility component $\chi_{yzy,as}$. We can calculate from the values in Table 1 that at the d_4-PET/uncured PDMS interface, $\chi_{ssp,as}/\chi_{sps,as} = \pm(0.47 \pm 0.06)$. The different Fresnel coefficients at the d_4-PET/PDMS interfaces in the ssp and sps polarization combinations were calculated. From Supporting Information, we have $\chi_{eff,ssp} = 1.48\chi_{yyz}$ and $\chi_{eff,sps} = 1.58\chi_{yzy}$. Therefore, $\chi_{yyz}/\chi_{yzy} = 1.07\chi_{eff,ssp}/\chi_{eff,sps}$. Using this relation, we can deduce at the d_4-PET/uncured PDMS interface $\chi_{yyz,as}/\chi_{yzy,as} = \pm(0.51 \pm 0.06)$. We can also calculate from the values listed in Table 1 that at the d_4-PET/cured PDMS interface, $\chi_{ssp,as}/\chi_{sps,as} = \pm(0.47 \pm 0.05)$. Similarly, we can deduce $\chi_{yyz,as}/\chi_{yzy,as} = \pm(0.51 \pm 0.05)$.

The values of $\chi_{yyz,s}/\chi_{yyz,as}$ and $\chi_{yyz,as}/\chi_{yzy,as}$ obtained in the experiments were compared to the calculated map shown in Figures 3c and 3d to deduce the possible angle range of the PDMS methyl group orientation. Considering the possible fitting errors and other experimental errors, a 20% error bar was included in the measured ratios for orientation analysis. The possible values for θ and ψ of Si(CH_3)$_2$ groups at the d_4-PET/PDMS interfaces were then plotted for each measurement and for both measurements (Figure 5). Figure 5 presents a set of heat map style plots to display all orientations for which calculated values fall within ±20% of the measured χ component ratios. The details on how to construct such heat maps have been reported.[60] Figure 5a shows that at the d_4-PET/uncured PDMS interface, according to $\chi_{yyz,s}/\chi_{yyz,as} = 1.24$ obtained before, Si(CH_3)$_2$ groups tend to have a >75° tilt angle,

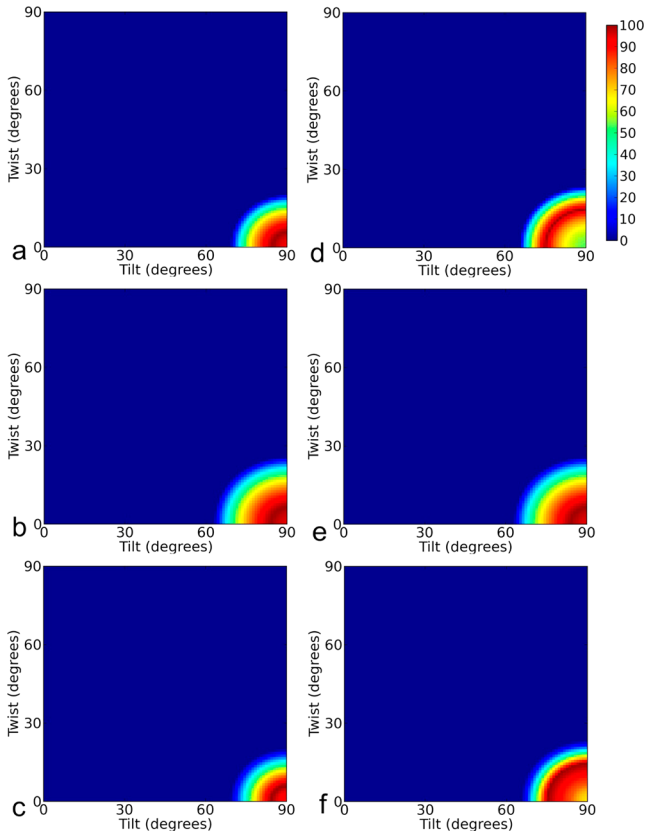

Figure 5. Plot $\chi_{yyz,s}/\chi_{yyz,as}$ and $\chi_{yyz,as}/\chi_{yzy,as}$ values obtained from SFG experiment in Figures 3c and 3d, respectively, to obtain: (a) Orientation range of Si(CH_3)$_2$ at the d_4-PET/uncured PDMS interface using $\chi_{yyz,s}/\chi_{yyz,as} = 1.24$. (b) Orientation range of Si(CH_3)$_2$ at the d_4-PET/uncured PDMS interface using $\chi_{yyz,as}/\chi_{yzy,as} = 0.51$. (d) Orientation range of Si(CH_3)$_2$ at the d_4-PET/cured PDMS interface using $\chi_{yyz,s}/\chi_{yyz,as} = 1.35$. (e) Orientation range of Si(CH_3)$_2$ at the d_4-PET/cured PDMS interface using $\chi_{yyz,as}/\chi_{yzy,as} = 0.51$. (c) Overlapping area of (a) and (b). (f) Overlapping area of (d) and (e).

but a <15° twist angle. On the basis of $\chi_{yyz,as}/\chi_{yzy,as} = 0.51$, it is deduced that the possible range shown in Figure 5b is larger. Possible values of tilt angles and twist angles are $\theta > 70°$ and $\psi < 20°$, respectively. The overlapping orientation angle region that satisfies both measurements is shown in Figure 5c, where the possible orientations for PDMS methyl groups are within the range of tilt angle >75° and twist angle <15°. Here $\chi_{yyz,as}/\chi_{yzy,as} = 0.51$ rather than −0.51 was chosen because the possible orientation angle range deduced from the negative value would not have any overlap with that obtained by $\chi_{yyz,s}/\chi_{yyz,as} = 1.24$ (Supporting Information). According to eqs 5−8, if the tilt angle is $\theta = 90°$, $\chi_{yyz,s} = \chi_{yyz,as} = \chi_{yzy,as} = 0$, there should be no SFG signals detected in the ssp and sps polarization combinations. However, SFG signals in both polarization combinations were detected, which indicates that $\theta > 75°$ but θ

dx.doi.org/10.1021/jp307472j | J. Phys. Chem. C 2013, 117, 3903−3914

≠ 90°. The tilt angles for PDMS methyl groups at the d_4-PET/uncured PDMS interface are large but not equal to 90°. At the same time, they tend to have very small twist angles at the interface.

Similarly, at the d_4-PET/cured PDMS interface, the possible orientation angle values derived by two different measurements ($\chi_{yyz,s}/\chi_{yyz,as}$ = 1.35 and $\chi_{yyz,as}/\chi_{yzy,as}$ = 0.51) are shown in Figures 5d and 5e. The overlapping area is shown in Figure 5f, which indicates a similar but slightly larger orientation range than that shown in Figure 5c. In the calculation, $\chi_{yyz,as}/\chi_{yzy,as}$ = 0.51 was used rather than $\chi_{yyz,as}/\chi_{yzy,as}$ = −0.51 also because only the positive value will lead to orientation angle range which can overlap with that obtained from the other measurement $\chi_{yyz,s}/\chi_{yyz,as}$ = 1.35 (Supporting Information). From Figure 5f, we can conclude at the d_4-PET/cured PDMS interface methyl groups tend to have big tilt angles (>70°) (but the tilt angles are not equal to 90°). The twist angles for the methyl groups are small (<20°).

SFG spectra from the silica/PDMS interface were collected before and after curing PDMS (Figure 6). Before curing, both

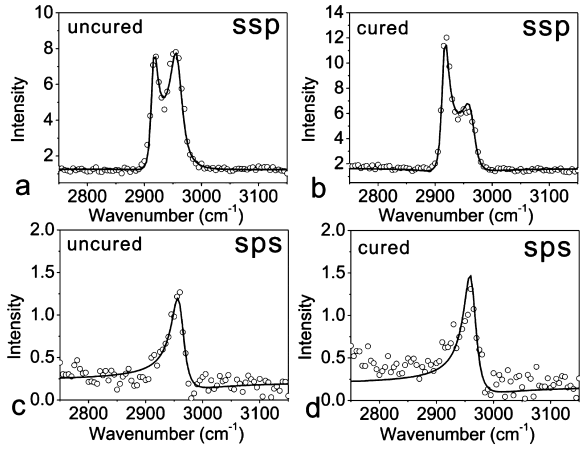

Figure 6. (a, c) The ssp/sps SFG spectra collected from the silica/PDMS interface before curing and (b, d) after curing. Dots are measured data; lines are fitting results.

the C−H symmetric and asymmetric stretching signals of Si−CH_3 could be detected in ssp polarization combination (Figure 6a), while in the sps spectrum, only the asymmetric stretching signal could be detected at around 2960 cm^{-1} (Figure 6c). For the ssp spectrum, good fitting results could only be achieved when opposite amplitude signs for the symmetric and asymmetric C−H stretching signals were used. This suggests that at the silica/PDMS interface the symmetric and asymmetric stretching modes of Si−CH_3 groups have different phases. The fitting results shown in Table 2 indicate that at silica/uncured PDMS interface, $\chi_{yyz,s}/\chi_{yyz,as}$ = −0.98 ± 0.13. The deduced orientation range of $Si(CH_3)_2$ groups based on this measurement is shown in Figure 7a. As Figure 5, the set of heat map style plots shown in Figure 7 also display all orientations

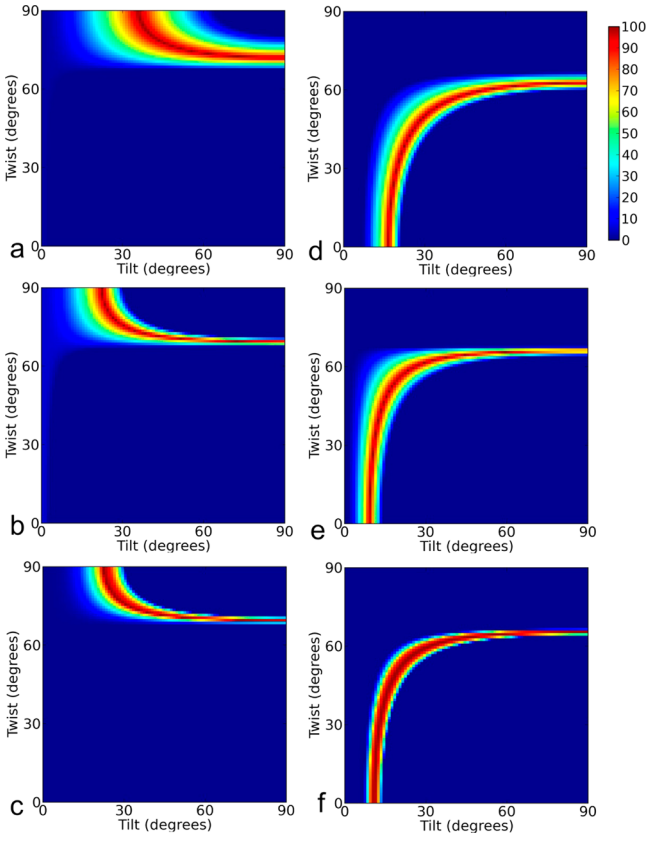

Figure 7. Plot $\chi_{yyz,s}/\chi_{yyz,as}$ and $\chi_{yyz,as}/\chi_{yzy,as}$ values obtained from SFG experiment in Figures 3c and 3d, respectively, to obtain: (a) Orientation range of $Si(CH_3)_2$ at the silica/uncured PDMS interface using $\chi_{yyz,s}/\chi_{yyz,as}$ = −0.98. (b) Orientation range of $Si(CH_3)_2$ at the silica/uncured PDMS interface using $\chi_{yyz,as}/\chi_{yzy,as}$ = −2.71. (d) Orientation range of $Si(CH_3)_2$ at the silica/cured PDMS interface using $\chi_{yyz,s}/\chi_{yyz,as}$ = −1.53. (e) Orientation range of $Si(CH_3)_2$ at the silica/cured PDMS interface using $\chi_{yyz,as}/\chi_{yzy,as}$ = −1.83. (c) Overlapping area of (a) and (b). (f) Overlapping area of (d) and (e).

for which calculated values fall within ±20% of the experimentally measured data. From the fitting results, we can also obtain $\chi_{ssp,as}/\chi_{sps,as}$ = ±(2.66 ± 0.30) at such interface. The different Fresnel coefficients at the silica/PDMS interfaces in the ssp and sps SFG signals were calculated. According to Supporting Information, $\chi_{eff,ssp}$ = 1.31χ_{yyz} and $\chi_{eff,sps}$ = 1.33χ_{yzy}. Therefore, χ_{yyz}/χ_{yzy} = 1.02$\chi_{eff,ssp}/\chi_{eff,sps}$. Accordingly, at the silica/uncured PDMS interface, $\chi_{yyz,as}/\chi_{yzy,as}$ = ±(2.71 ± 0.31). If the positive value of 2.71 was chosen, then there will be no possible orientation range satisfied (Supporting Information). Therefore, $\chi_{yyz,as}/\chi_{yzy,as}$ = −2.71 was used in calculation. The

Table 2. Spectral Fitting Results for the SFG Spectra Shown in Figure 6

interfaces	ω_q (cm^{-1})	A_q	Γ_q (cm^{-1})	$\lvert A_q/\Gamma_q \rvert$	assignment
silica/PDMS (uncured, ssp)	2915	17.2 ± 0.8	6.9 ± 0.7	2.49 ± 0.28	Si−CH_3(s)
	2958	−33.6 ± 1.2	13.3 ± 0.9	2.53 ± 0.19	Si−CH_3(as)
silica/PDMS (cured, ssp)	2917	22.9 ± 1.3	7.5 ± 0.7	3.05 ± 0.33	Si−CH_3(s)
	2964	−26.1 ± 1.4	13.1 ± 0.8	1.99 ± 0.16	Si−CH_3(as)
silica/PDMS (uncured, sps)	2960	12.7 ± 0.7	13.3 ± 0.9	0.95 ± 0.08	Si−CH_3(as)
silica/PDMS (cured, sps)	2962	14.5 ± 1.0	13.1 ± 0.9	1.11 ± 0.11	Si−CH_3(as)

dx.doi.org/10.1021/jp307472j | J. Phys. Chem. C 2013, 117, 3903−3914

possible orientation range deduced based on this measurement is shown in Figure 7b. The overlapping orientation range which satisfies both measurements is shown in Figure 7c. At the silica/PDMS interface, the possible methyl group tilt angles and twist angles covered a broad range. The range was quite different from that of methyl groups at the d_4-PET/PDMS interface due to the different interfacial interactions. Here the twist angle tended to be bigger than 60°, which was much larger than that at d_4-PET/PDMS interface. Similarly, θ cannot be 90°. Otherwise, there would not be SFG signal detected.

Fitting results from the SFG spectra collected from the silica/cured PDMS interface (Figure 6b,d and Table 2) show that $\chi_{yyz,s}/\chi_{yyz,as} = -1.53 \pm 0.21$ and $\chi_{ssp,as}/\chi_{sps,as} = \pm(1.79 \pm 0.23)$. Considering the different Fresnel coefficients in the ssp and sps SFG signals, we can obtain $\chi_{yyz,as}/\chi_{yzy,as} = \pm(1.83 \pm 0.23)$. Similarly, the possibility that $\chi_{yyz,as}/\chi_{yzy,as}$being $+(1.83 \pm 0.23)$ can be excluded (Supporting Information) and $\chi_{yyz,as}/\chi_{yzy,as} = -1.83$ was used in calculation. The possible orientation range of methyl groups at the interface deduced from each measurement is shown in Figures 7d and 7e, respectively. The overlapping range which satisfies both measurements is shown in Figure 7f and can be considered as possible orientation range of methyl groups at the silica/PDMS interface after curing.

Figure 7 shows that the possible orientation ranges of PDMS methyl groups at silica/PDMS interfaces are broad. In order to narrow down the possible orientation ranges at such interfaces, the resonance strengths $\chi_{yyz,s}$ and $\chi_{yyz,as}$ of PDMS methyl groups at the d_4-PET/PDMS and silica/PDMS interfaces were also compared. From Figure 5 it was concluded that PDMS methyl groups tend to have big tilt angle between 77° and 90° and small twist angle between 0° and 13° (50% maximum) at the d_4-PET/PDMS interface before curing. This corresponds to the area of $0 < \chi_{yyz,s,(uncured)PDMS/dPET}\varepsilon_0/N < 0.70$ in Figure 3a. Possible values of $\chi_{yyz,s,(uncured)PDMS/silica}\varepsilon_0/N$ at the PDMS/silica interfaces were obtained by comparing its symmetric C−H stretching resonance strength with that at the d_4-PET/uncured PDMS interface. Since different interfaces were studied, different Fresnel coefficients also need to be considered. According to the spectral fitting results, PDMS methyl group symmetric C−H stretching signal detected from the silica/uncured PDMS interface was $\chi_{ssp,s,(uncured)PDMS/silica} = 2.49 \pm 0.28$ (Table 2, in arbitrary unit). At the d_4-PET/uncured PDMS interface, the methyl group C−H symmetric stretching signal strength was $\chi_{ssp,s,(uncured)PDMS/dPET} = 1.22 \pm 0.12$ (in arbitrary unit). According to calculation, the Fresnel coefficients were different at the silica/PDMS and PET/PDMS interfaces (Supporting Information). Furthermore, compared to the silica/PDMS interface, IR and visible beams reaching the d_4-PET/PDMS interface were attenuated by silica/d_4-PET interface due to the reflection. Combining Fresnel coefficient and attenuation factor (Supporting Information), $(\chi_{yyz,s,(uncured)PDMS/silica}/\chi_{yyz,s,(uncured)PDMS/dPET}) = 1.03$ $(\chi_{ssp,s,(uncured)PDMS/silica}/\chi_{ssp,s,(uncured)PDMS/dPET})$. Therefore, applying two measured values, we can obtain $(\chi_{yyz,s,(uncured)PDMS/silica}/\chi_{yyz,s,(uncured)PDMS/dPET}) = 2.10$. Since $0 < \chi_{yyz,s,(uncured)PDMS/dPET}\varepsilon_0/N < 0.70$, therefore we have $0 < \chi_{yyz,s,(uncured)PDMS/silica}\varepsilon_0/N < 1.47$. The possible orientation range with $0 < \chi_{yyz,s,(uncured)PDMS/silica}\varepsilon_0/N < 1.47$ in Figure 3a was overlapped with the range deduced in Figure 7c. The possible orientation range of methyl group at silica/uncured PDMS interface is shown in Figure 8a and is narrowed to 45°−90° in tilt angle and 70°−75° in twist angle. Again, Figure 8 presents a set of heat map style plots to display all orientations for which calculated values fall within ±20% of the measured data.

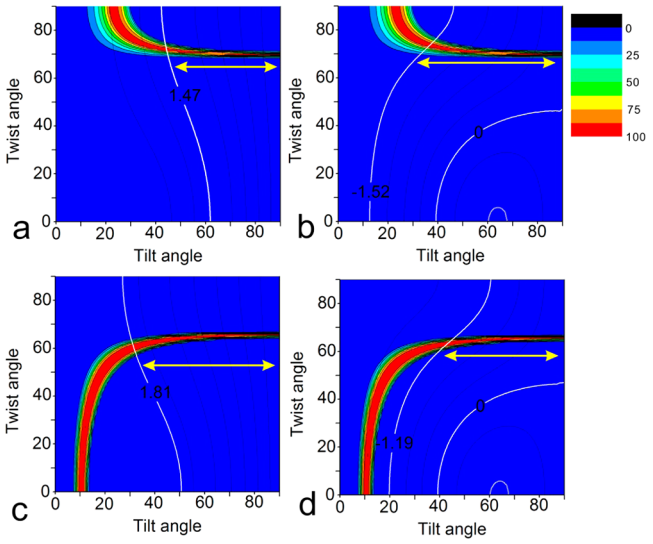

Figure 8. Possible orientation range of $Si(CH_3)_2$ group at silica/uncured PDMS interface further determined using (a) $(\chi_{yyz,s,(uncured)PDMS/silica}/\chi_{yyz,s,(uncured)PDMS/dPET})$ and (b)-$(\chi_{yyz,as,(uncured)PDMS/silica}/\chi_{yyz,as,(uncured)PDMS/dPET})$. Possible orientation range of $Si(CH_3)_2$ group at silica/cured PDMS interface further determined using (c) $(\chi_{yyz,s,(cured)PDMS/silica}/\chi_{yyz,s,(uncured)PDMS/dPET})$ and (d) $(\chi_{yyz,as,(cured)PDMS/silica}/\chi_{yyz,as,(uncured)PDMS/dPET})$. For (a) and (c), possible ranges are from white curve to the right; for (b) and (d), possible ranges are between two white lines. Arrows are used to demonstrate the possible ranges in all figures.

This analysis can be further validated by comparing the asymmetric C−H stretching signals. From Tables 1 and 2, the signal strengths of the asymmetric C−H stretching modes at the d_4-PET/uncured PDMS interface and the silica/uncured PDMS interface were 0.98 ± 0.09 and 2.53 ± 0.19, respectively (in arbitrary units). Therefore, the signal strength ratio was $\chi_{ssp,as,(uncured)PDMS/silica}/\chi_{ssp,as,(uncured)PDMS/dPET} = -(2.53/0.98) = -2.58$. The negative sign used here indicates that at these two interfaces, the asymmetric C−H stretches have different signs compared to the corresponding symmetric C−H stretches, as mentioned previously. We can further calculate the ratio $\chi_{yyz,as,(uncured)PDMS/silica}/\chi_{yyz,as,(uncured)PDMS/dPET} = 1.03 \times (-2.58) = -2.66$. At the d_4-PET/uncured PDMS interface the methyl group tilt angle was determined to be between 77° and 90° and twist angle was between 0 and 13°, which corresponds to the area of $0 < \chi_{yyz,as,(uncured)PDMS/dPET}\varepsilon_0/N < 0.57$ in Figure 3b. At the silica/uncured PDMS interface, the value $\chi_{yyz,as,(uncured)PDMS/dPET}\varepsilon_0/N$ needs to be multiplied by the factor of −2.66, and thus $-1.52 < \chi_{yyz,as,(uncured)PDMS/silica}\varepsilon_0/N < 0$. The corresponding range in Figure 3b was plotted together with possible orientations determined in Figure 7c and is shown as Figure 8b. The possible methyl group orientation at the silica/uncured PDMS interface is $35° < \theta < 90°$ in tilt angle and 70°−75° in twist angle. This is not very different from the result obtained by comparing the C−H symmetric stretching signals (Figure 8a), but with a slightly larger range. In summary, Figure 8a demonstrates the most possible orientation angle range of methyl groups at the silica/uncured PDMS interface.

The same analysis can also be applied to the silica/cured PDMS interface. From Tables 1 and 2 considering C−H symmetric mode, $\chi_{ssp,s,(cured)PDMS/silica}/\chi_{ssp,s,(uncured)PDMS/dPET} = 3.05/1.22 = 2.50$. Therefore, we can obtain

dx.doi.org/10.1021/jp307472j | J. Phys. Chem. C 2013, 117, 3903−3914

$\chi_{yyz,s,(cured)PDMS/silica}/\chi_{yyz,s,(uncured)PDMS/dPET}$ = 1.03 × 2.50 = 2.58. For d_4-PET/uncured PDMS interface, 0 < $\chi_{yyz,s,(uncured)PDMS/dPET}\varepsilon_0/N$ < 0.70. Therefore, 0 < $\chi_{yyz,s,(cured)PDMS/silica}\varepsilon_0/N$ < 1.81 corresponds to range 0–1.81 in Figure 3a. The overlapped area of Figure 3a (0–1.81) and Figure 7f is shown in Figure 8c. The results suggesting possible orientation range of methyl group at silica/cured PDMS interface can be narrowed down to tilt angle 33°–90° and twist angle 58°–66°. Similarly, using the asymmetric C–H stretching mode, $\chi_{ssp,as,(cured)PDMS/silica}/\chi_{ssp,as,(uncured)PDMS/dPET}$ = −(1.99/0.98) = −2.03. This further gives $\chi_{yyz,as,(cured)PDMS/silica}/\chi_{yyz,as,(uncured)PDMS/dPET}$ = 1.03 × (−2.03) = −2.09. For the d_4-PET/uncured PDMS interface, 0 < $\chi_{yyz,as,(uncured)PDMS/dPET}\varepsilon_0/N$ < 0.57. Therefore, −1.19 < $\chi_{yyz,as,(cured)PDMS/silica}\varepsilon_0/N$ < 0 corresponds to −1.19 to 0 in Figure 3b. The overlapped area of Figure 3b (0 to −1.19) and Figure 7f is shown in Figure 8d. The orientation ranges obtained in Figures 8c and 8d are quite similar, while the latter has a slightly smaller range, tilt angle 45°–90° and twist angle 60°–66°. This suggest that the methyl group's possible orientation range at the silica/cured PDMS interface is 45°–90° in tilt angle and 60°–66° in twist angle.

A single methyl group possesses a C_{3v} symmetry; therefore, it is usually not necessary to consider the twist angle. In the above analysis, for a $Si(CH_3)_2$ group, we considered both tilt and twist angles. Here we demonstrate that the consideration of twist angle is essential. Figure 9 shows the ratios of $\chi_{yyz,s}/\chi_{yyz,as}$ and

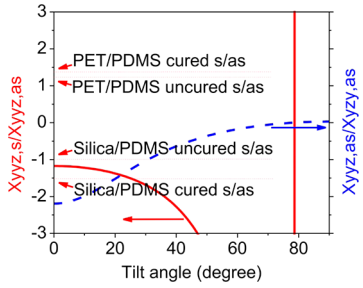

Figure 9. $\chi_{yyz,s}/\chi_{yyz,as}$ (solid red line) and $\chi_{yyz,as}/\chi_{yzy,as}$ (broken blue line) as functions of tilt angle (the ratio values are obtained by averaging twist angle ψ from 0 to 360°). The experimentally measured values are shown as dotted lines and demonstrated by the red arrows.

$\chi_{yyz,as}/\chi_{yzy,as}$ as functions of the tilt angle θ after averaging the twist angle from 0 to 360°. It shows that $\chi_{yyz,s}/\chi_{yyz,as}$ cannot have a reasonable positive value for the tilt angle between 0 and 90°. From the experiment we obtained that $\chi_{ssp,s}/\chi_{ssp,as}$ = $\chi_{yyz,s}/\chi_{yyz,as}$ = 1.24 and 1.35 respectively for PDMS methyl groups at the d_4-PET/PDMS interfaces before and after curing PDMS. These two values are both positive. This indicates that the twist angle of $Si(CH_3)_2$ groups at the d_4-PET/PDMS interfaces cannot be averaged. $Si(CH_3)_2$ groups tend to adopt certain twist angles (e.g., <15° at the d_4-PET/PDMS interfaces as discussed before) rather than adopt all possible twist angles from 0 to 90°. Similarly, at the silica/uncured PDMS interface, Figure 9 shows that the measured $\chi_{yyz,s}/\chi_{yyz,as}$ = −0.98 ratio is out of the possible range, indicating that at this interface the twist angle for $Si(CH_3)_2$ groups cannot be averaged. At the silica/cured PDMS interface, even though both the measured $\chi_{yyz,s}/\chi_{yyz,as}$ = −1.53 and $\chi_{yyz,as}/\chi_{yzy,as}$ = −1.83 (not shown in Figure 9) ratios fall on the corresponding curve after averaging the twist angle, but the possible tilt angles deduced from these two measurements are not the same, at ∼28° and ∼18°, respectively. We believe that this is also because the twist angles cannot be averaged.

As we showed in Table 1, the best fitting results for ssp SFG spectra collected from the d_4-PET/PDMS interfaces were obtained when the strengths or amplitudes of the symmetric and asymmetric C–H stretching signals have the same sign. Differently, Table 2 shows that the best fitting results for ssp SFG spectra collected from the silica/PDMS interfaces were obtained when the amplitudes of the symmetric and asymmetric C–H stretching signals have different signs. To further confirm the spectral fitting results, silica prisms coated with a thin TiO_2 film were used in the experiment to provide nonresonant SFG signals. Such nonresonant signals can interfere with the SFG signals generated from the PDMS methyl groups at the interfaces to determine the relative signs (or phases) of the SFG signals.

Similar to the previous d_4-PET/PDMS interface, a d_4-PET film with a thickness of about 50 nm was spin-cast on the TiO_2 film (deposited on fused silica prism) at the spin speed of ∼2500 rpm and using a 2 wt % d_4-PET solution in 2-chlorophenol. Then the d_4-PET surface was contacted with PDMS, and SFG spectra were collected from this interface. The SFG spectrum collected from the d_4-PET/PDMS interface before curing is shown in Figure 10a. Two peaks at ∼2900 and

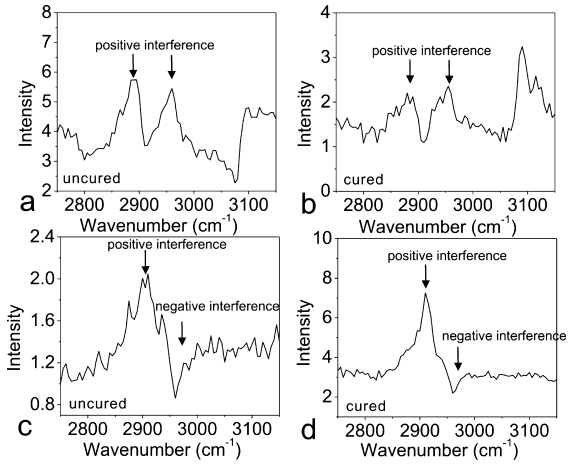

Figure 10. SFG spectra collected from the d_4-PET/PDMS interface (d_4-PET on a TiO_2 layer): (a) before curing, (b) after curing. SFG spectra collected from the silica/PDMS interface (a thin layer of silica on a TiO_2 layer): (c) before curing, (d) after curing.

∼2960 cm^{-1} were detected, both of which had positive amplitudes relative to the nonresonant background. This demonstrated that these two peaks have the same phase (or their amplitudes have the same sign). After curing PDMS, the ssp SFG spectrum collected from the d_4-PET/cured PDMS interface is shown in Figure 10b, which leads to the similar conclusion that the peaks at ∼2900 and ∼2960 cm^{-1} have the same phase. Therefore, the results obtained with the help of a thin TiO_2 film are compatible to those discussed previously, validating the previous fitting results.

A thin layer of SiO_2 film with a thickness of 50 nm was also coated on the TiO_2 film (deposited on a fused silica prism). SFG ssp spectra were then collected from the SiO_2 (on TiO_2)/PDMS interface. Before curing PDMS, the detected SFG spectrum had one positive and one negative interference (at 2905 and 2960 cm^{-1}) with the nonresonant SFG background generated from the TiO_2 film (Figure 10c). This indicates that

dx.doi.org/10.1021/jp307472j | J. Phys. Chem. C 2013, 117, 3903–3914

the symmetric and asymmetric C−H stretching signals of the PDMS methyl groups at the silica/PDMS interface have different phases (the amplitudes of which have different signs). After curing PDMS, the SFG ssp spectrum was also collected from the interface (Figure 10d), which indicates the different phases for the symmetric and asymmetric C−H stretching signals of the methyl groups as well. These results also match the spectral fitting results discussed above. As shown in Figures 3c and 3d, different phases of the symmetric and asymmetric C−H stretches are related to different possible orientation ranges of $Si(CH_3)_2$ groups. Therefore, different phases detected at the PDMS/silica and PDMS/d_4-PET interfaces indicate that the possible orientations of $Si(CH_3)_2$ groups are different at the two interfaces.

Figure 10 shows that in all the SFG spectra the C−H symmetric stretching signals interfered with the TiO_2 nonresonant SFG signal similarly (positive interference), which suggests that methyl groups at both d_4-PET/PDMS and silica/PDMS interfaces before and after curing PDMS have the same absolute orientation. Since silica has a very hydrophilic surface, hydrophobic methyl groups may orient away from the silica surface (toward the bulk PDMS). The results further indicate that at the d_4-PET/PDMS interface the methyl groups may also orient away from the polymer surface. This is possible because C═O groups were detected on the PET surface,[61] showing that the PET surface can be hydrophilic (at least in some regions). Apparently the PET surface is less hydrophilic compared to the silica surface. This may account for the methyl groups with larger tilt angles at the d_4-PET/PDMS interface compared to that at the silica/PDMS interface.

To further confirm the conclusion regarding the absolute orientation of the methyl groups at the d_4-PET/PDMS and silica/PDMS interfaces, the absolute orientations of PDMS methyl groups at hydrophobic surfaces were studied. d_8-PS and d_8-PMMA were used to make hydrophobic surfaces. About 50 nm thin films of d_8-PS and d_8-PMMA on TiO_2 films were prepared using spin-coating. SFG ssp spectra were then collected from the d_8-PS/PDMS interface and the d_8-PMMA/PDMS interface before and after curing PDMS (Figure 11). The results show that the SFG signals detected from the C−H symmetric stretching modes of the PDMS methyl groups at the

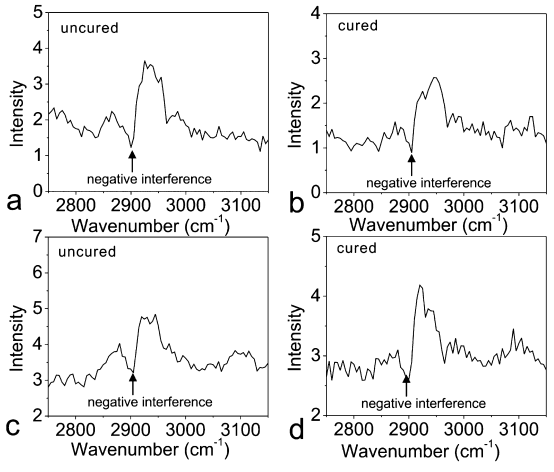

Figure 11. SFG spectra collected from the d_8-PS/PDMS interface (d_8-PS on a TiO_2 layer): (a) before curing, (b) after curing. SFG spectra collected from the d_8-PMMA/PDMS interface (d_8-PMMA on a TiO_2 layer): (c) before curing, (d) after curing.

d_8-PS/PDMS interface and d_8-PMMA/PDMS interface interfere differently with the nonresonant SFG signal from the TiO_2 film compared to the d_4-PET and silica cases discussed above. Figure 11 demonstrates that all the SFG signals from the PDMS methyl C−H symmetric stretches interfere negatively with the TiO_2 nonresonant background. This indicates that the absolute orientations of the PDMS methyl groups at the d_8-PS/PDMS interface and the d_8-PMMA/PDMS interface are different (opposite) compared to that at the d_4-PET/PDMS and silica/PDMS interfaces. This suggests that at the d_8-PS/PDMS and d_8-PMMA/PDMS interfaces, the methyl groups orient toward the d_8-PS and d_8-PMMA surfaces, respectively.

The different absolute orientations of PDMS methyl groups at buried interfaces can be explained according to the hydrophobicity of different surfaces. The water contact angles were measured on various surfaces which were used in this research to contact PDMS (Table 3). Silica had the smallest

Table 3. Contact Angle Measurement Results of Polymer and Silica Surfaces Used in the Experiment

material	d_4-PET	silica	d_8-PMMA	d_8-PS
av contact angle (deg)	62.8 ± 0.7	∼0	65.2 ± 0.6	88.3 ± 0.7

contact angle, while d_4-PET had a slightly smaller contact angle than d_8-PMMA and d_8-PS had the biggest contact angle. Therefore, the hydrophobic order of various surfaces is d_8-PS > d_8-PMMA > d_4-PET > silica. From the previous discussion, PDMS methyl groups at the d_4-PET/PDMS and silica/PDMS interfaces both orient away from the contacting media and toward the PDMS bulk. This is understandable because at the silica/PDMS interface, due to the unfavorable interactions between the methyl groups and hydrophilic silica, the methyl groups orient away from the silica surface. At the d_4-PET/PDMS interface, the deduced orientation of the interfacial $Si(CH_3)_2$ groups has large tilt angles. This indicates that the hydrophobicity of the d_4-PET surface is on the margin of determining the net orientation of PDMS methyl group orienting away or toward the contacting medium. At the d_8-PMMA/PDMS and d_8-PS/PDMS interfaces, the polymer surface hydrophobicity increases. Therefore, the methyl groups have more favorable interactions with the polymer surfaces. This leads to the net orientation of methyl groups tilting toward the polymer substrates.

In summary, at the silica/PDMS interface, the methyl groups tend to adopt different orientations compared to that at the d_4-PET/PDMS interface. At the d_4-PET/PDMS interface, $Si(CH_3)_2$ groups tend to have large tilt angles with small twist angles. A schematic representation of the possible orientations is shown in Figure 12. Even though the principal axis of the

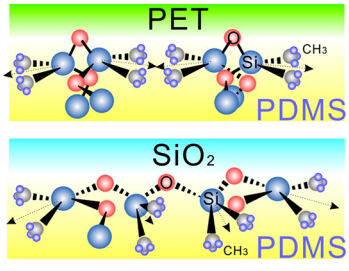

Figure 12. Schematic representations of PDMS molecules at PET and silica interfaces.

dx.doi.org/10.1021/jp307472j | J. Phys. Chem. C 2013, 117, 3903−3914

$Si(CH_3)_2$ group at the interface points to the PDMS bulk, it is possible that one methyl group points to the PET surface, while the other methyl group points to PDMS. This is understandable because PET is not very hydrophilic. There can be some hydrophobic areas on PET surface which can favorably interact with methyl groups. At the silica/PDMS interface before curing, methyl group tilt angle tends to be bigger than 45° with twist angle 70°−75°. After curing, the tilt angle is bigger than 45°, while the twist angle is 60°−66°. At both interfaces, methyl groups tend to orient toward the PDMS bulk due to the hydrophilic substrate surface. A schematic representation of PDMS at silica interfaces is also shown in Figure 12. At the PDMS/silica interface, both methyl groups point to the PDMS bulk while two oxygen atoms point to silica. This is hypothesized due to the hydrophilic nature of the fused silica surface.

5. CONCLUSION

The molecular structures at the buried d_4-PET/PDMS and silica/PDMS interfaces were measured. The results show that PDMS $Si(CH_3)_2$ groups tend to have different orientations at different interfaces. At the d_4-PET/PDMS interface, PDMS $Si(CH_3)_2$ groups tend to have large tilt angles (>70°) but small twist angles (<20°). The C−H symmetric and asymmetric stretching signals of PDMS methyl groups have the same phase. On the other hand, at the silica/PDMS interface, PDMS methyl groups tend to have a broader orientation range. Before and after curing PDMS, PDMS methyl group orientation does not have a significant change at the d_4-PET/PDMS interface (tilt angle >70°), while at the silica/PDMS interface, the twist angles changed about 10°. In this research we assumed a δ-orientation distribution of methyl groups at interfaces. In reality, the δ-distribution may not be accurate, but the deduced orientation angles should be sufficient to address the average orientations. We also conclude that it is necessary to consider the twist angles of PDMS methyl groups at buried interfaces. That is to say, PDMS methyl groups do not have a random distribution of twist angles. With the help of the nonresonant SFG signals generated from a TiO_2 thin film, it was confirmed that the methyl group symmetric and asymmetric stretching modes have the same phase at the d_4-PET/PDMS interface and have different phases at the silica/PDMS interface, both before and after curing. PDMS methyl groups tend to orient toward the PDMS bulk rather than toward the d_4-PET or silica substrates. Differently, when PDMS materials are in contact with hydrophobic surfaces, such as d_8-PS and d_8-PMMA, the PDMS methyl groups orient to the hydrophobic surfaces due to the favorable interactions at the interfaces.

■ ASSOCIATED CONTENT

Supporting Information

Further discussions on refractive index, Fresnel coefficient, and possible orientation angle range. This material is available free of charge via the Internet at http://pubs.acs.org.

■ AUTHOR INFORMATION

Corresponding Author

*E-mail zhanc@umich.edu; Fax 734-647-4865.

Notes

The authors declare no competing financial interest.

■ ACKNOWLEDGMENTS

This work was supported by the Semiconductor Research Corporation (P13696). The authors want to thank Andrew Boughton for the help of Python Software, Fugen Wu for the help of coating TiO_2 and silica films, and John Myers for the help in proofreading the article.

■ REFERENCES

(1) Kinloch, A. J. *Adhesion and Adhesives: Science and Technology*; Chapman and Hall: London, 1987.
(2) Yacobi, B. G.; Martin, S.; Davis, K.; Hudson, A.; Hubert, M. Adhesive Bonding in Microelectronics and Photonics. *J. Appl. Phys.* **2002**, *91*, 6227−6262.
(3) Mine, K.; Nishio, M.; Sumimura, S. Heat Curable Organopolysiloxane Compositions Containing Adhesion Additives. U.S. Patent 4,033,924, July 5, 1977.
(4) Schulz, J. R. Self-Adhering Silicone Compositions and Preparations Thereof. U.S. Patent 4,087,585, May 2, 1978.
(5) Gray, T. E.; Lutz, M. A. Curable Organopolysiloxane Compositions with Improved Adhesion. U.S. Patent 5,595,826, Jan 21, 1997.
(6) Brown, H. R. Chain Pullout and Mobility Effects in Friction and Lubrication. *Science* **1994**, *263*, 1411−1413.
(7) Dai, C. A.; Dair, B. J.; Dai, K. H.; Ober, C. K.; Kramer, E. J.; Hui, C. Y.; Jelinski, L. W. Reinforcement of Polymer Interfaces with Random Copolymers. *Phys. Rev. Lett.* **1994**, *73*, 2472−2475.
(8) Edgecombe, B. D.; Stein, J. A.; Fréchet, J. M. J.; Xu, Z.; Kramer, E. J. The Role of Polymer Architecture in Strengthening Polymer-Polymer Interfaces: A Comparison of Graft, Block, and Random Copolymers Containing Hydrogen-Bonding Moieties. *Macromolecules* **1998**, *31*, 1292−1304.
(9) Schulze, J. S.; Moon, B.; Lodge, T. P.; Macosko, C. W. Measuring Copolymer Formation from End-Functionalized Chains at a PS/PMMA Interface Using FRES and SEC. *Macromolecules* **2001**, *34*, 200−205.
(10) Shen, Y. R. *The Principles of Nonlinear Optics*; J. Wiley: New York, 1984.
(11) Shen, Y. R. Surface Properties Probed by Second-Harmonic and Sum-Frequency Generation. *Nature* **1989**, *337*, 519−525.
(12) Zhuang, X.; Miranda, P.; Kim, D.; Shen, Y. R. Mapping Molecular Orientation and Conformation at Interfaces by Surface Nonlinear Optics. *Phys. Rev. B* **1999**, *59*, 12632−12640.
(13) Chen, Z.; Shen, Y. R.; Somorjai, G. A. Studies of Polymer Surfaces by Sum Frequency Generation Vibrational Spectroscopy. *Annu. Rev. Phys. Chem.* **2002**, *53*, 437−465.
(14) Chen, C. Y.; Wang, J.; Even, M. A.; Chen, Z. Sum Frequency Generation Vibrational Spectroscopy Studies on "Buried" Polymer/Polymer Interfaces. *Macromolecules* **2002**, *35*, 8093−8097.
(15) Loch, C. L.; Ahn, D.; Chen, C.; Chen, Z. Polymer-Silane Interactions Probed by Sum Frequency Generation Vibrational Spectroscopy. *J. Adhes.* **2005**, *81*, 319−345.
(16) Kweskin, S. J.; Komvopoulos, K.; Somorjai, G. A. Molecular Restructuring at Poly(n-butyl methacrylate) and Poly(methyl methacrylate) Surfaces due to Compression by a Sapphire Prism Studied by Infrared-Visible Sum Frequency Generation Vibrational Spectroscopy. *Langmuir* **2005**, *21*, 3647−3652.
(17) Moad, A. J.; Simpson, G. J. Self-Consistent Approach for Simplifying the Molecular Interpretation of Nonlinear Optical and Multiphoton Phenomena. *J. Phys. Chem. A* **2005**, *109*, 1316−1323.
(18) Chen, Z. Understanding Surfaces and Buried Interfaces of Polymer Materials at the Molecular Level Using Sum Frequency Generation Vibrational Spectroscopy. *Polym. Int.* **2007**, *56*, 577−587.
(19) Fourkas, J. T.; Walker, R. A.; Can, S. Z.; Gershgoren, E. Effects of Reorientation in Vibrational Sum-Frequency Spectroscopy. *J. Phys. Chem. C* **2007**, *111*, 8902−8915.
(20) Buch, V.; Tarbuck, T.; Richmond, G. L.; Groenzin, H.; Li, I.; Shultz, M. J. Sum Frequency Generation Surface Spectra of Ice, Water,

and Acid Solution Investigated by an Exciton Model. *J. Chem. Phys.* **2007**, *127*, 204710.
(21) Lu, X. L.; Shephard, N.; Han, J. L.; Xue, G.; Chen, Z. Probing Molecular Structures of Polymer/Metal Interfaces by Sum Frequency Generation Vibrational Spectroscopy. *Macromolecules* **2008**, *41*, 8770−8777.
(22) Baldelli, S. Surface Structure at the Ionic Liquid-Electrified Metal Interface. *Acc. Chem. Res.* **2008**, *41*, 421−431.
(23) Sovago, M.; Vartiainen, E.; Bonn, M. Observation of Buried Water Molecules in Phospholipid Membranes by Surface Sum-Frequency Generation Spectroscopy. *J. Chem. Phys.* **2009**, *131*, 161107.
(24) Geiger, F. M. Second Harmonic Generation, Sum Frequency Generation, and Chi(3): Dissecting Environmental Interfaces with a Nonlinear Optical Swiss Army knife. *Annu. Rev. Phys. Chem.* **2009**, *60*, 61−83.
(25) Chen, Z. Investigating Buried Polymer Interfaces Using Sum Frequency Generation Vibrational Spectroscopy. *Prog. Polym. Sci.* **2010**, *35*, 1376−1402.
(26) Lu, X. L.; Clarke, M. L.; Li, D. W.; Wang, X. P.; Xue, G.; Chen, Z. A Sum Frequency Generation Vibrational Study of the Interference Effect in Poly(n-butyl methacrylate) Thin Films Sandwiched between Silica and Water. *J. Phys. Chem. C* **2011**, *115*, 13759−13767.
(27) Zhang, C.; Shephard, N. E.; Rhodes, S. M.; Chen, Z. Headgroup Effect on Silane Structures at Buried Polymer/Silane and Polymer/Polymer Interfaces and Their Relations to Adhesion. *Langmuir* **2012**, *28*, 6052−6059.
(28) Zhang, C.; Chen, Z. Quantitative Molecular Level Understanding of Ethoxysilane at Poly(dimethylsiloxane)/Polymer Interfaces. *Langmuir* **2013**, *29*, 610−619.
(29) Hirose, C.; Akamatsu, N.; Domen, K. Formulas for the Analysis of the Surface SFG Spectrum and Transformation Coefficients of Cartesian SFG Tensor Components. *Appl. Spectrosc.* **1992**, *46*, 1051−1072.
(30) Hirose, C.; Akamatsu, N.; Domen, K. Formulas for the Analysis of Surface Sum-Frequency Generation Spectrum by CH Stretching Modes of Methyl and Methylene Groups. *J. Chem. Phys.* **1992**, *96*, 997−1004.
(31) Gautam, K. S.; Schwab, A. D.; Dhinojwala, A.; Zhang, D.; Dougal, S. M.; Yeganeh, M. S. Molecular Structure of Polystyrene at Air/Polymer and Solid/Polymer Interfaces. *Phys. Rev. Lett.* **2000**, *85*, 3854−3857.
(32) Wang, J.; Chen, C.; Buck, S. M.; Chen, Z. Molecular Chemical Structure on Poly(methyl methacrylate) (PMMA) Surface Studied by Sum Frequency Generation (SFG) Vibrational Spectroscopy. *J. Phys. Chem. B* **2001**, *105*, 12118−12125.
(33) Wang, J.; Lee, S. H.; Chen, Z. Quantifying the Ordering of Adsorbed Proteins in Situ. *J. Phys. Chem. B* **2008**, *112*, 2281−2290.
(34) Zhang, D.; Ward, R. S.; Shen, Y. R.; Somorjai, G. A. Environment-Induced Surface Structural Changes of a Polymer: An in situ IR+ Visible Sum-Frequency Spectroscopic Study. *J. Phys. Chem. B* **1997**, *101*, 9060−9064.
(35) Chen, C.; Wang, J.; Chen, Z. Surface Restructuring Behavior of Various Types of Poly(dimethylsiloxane) in Water Detected by SFG. *Langmuir* **2004**, *20*, 10186−10193.
(36) Yurdumakan, B.; Nanjundiah, K.; Dhinojwala, A. Origin of Higher Friction for Elastomers Sliding on Glassy Polymers. *J. Phys. Chem. C* **2007**, *111*, 960−965.
(37) Yurdumakan, B.; Harp, G. P.; Tsige, M.; Dhinojwala, A. Template-Induced Enhanced Ordering under Confinement. *Langmuir* **2005**, *21*, 10316−10319.
(38) Ye, H.; Gu, Z.; Gracias, D. H. Kinetics of Ultraviolet and Plasma Surface Modification of Poly(dimethylsiloxane) Probed by Sum Frequency Vibrational Spectroscopy. *Langmuir* **2006**, *22*, 1863−1868.
(39) Kim, C.; Gurau, M. C.; Cremer, P. S.; Yu, H. Chain Conformation of Poly(dimethyl siloxane) at the Air/Water Interface by Sum Frequency Generation. *Langmuir* **2008**, *24*, 10155−10160.
(40) Ye, S.; McClelland, A.; Majumdar, P.; Stafslien, S. J.; Daniels, J.; Chisholm, B.; Chen, Z. Detection of Tethered Biocide Moiety Segregation to Silicone Surface Using Sum Frequency Generation Vibrational Spectroscopy. *Langmuir* **2008**, *24*, 9686−9694.
(41) Ye, S.; Majumdar, P.; Chisholm, B.; Stafslien, S.; Chen, Z. Antifouling and Antimicrobial Mechanism of Tethered Quaternary Ammonium Salts in a Cross-Linked Poly(dimethylsiloxane) Matrix Studied Using Sum Frequency Generation Vibrational Spectroscopy. *Langmuir* **2010**, *26*, 16455−16462.
(42) Shi, Q.; Ye, S.; Spanninga, S. A.; Su, Y.; Jiang, Z.; Chen, Z. The Molecular Surface Conformation of Surface-Tethered Polyelectrolytes on PDMS Surfaces. *Soft Matter* **2009**, *5*, 3487−3494.
(43) Chen, C. Y.; Loch, C. L.; Wang, J.; Chen, Z. Different Molecular Structures at Polymer/Silane Interfaces Detected by SFG. *J. Phys. Chem. B* **2003**, *107*, 10440−10445.
(44) Loch, C. L.; Ahn, D.; Chen, Z. Sum Frequency Generation Vibrational Spectroscopic Studies on a Silane Adhesion-Promoting Mixture at a Polymer Interface. *J. Phys. Chem. B* **2006**, *110*, 914−918.
(45) Loch, C. L.; Ahn, D.; Vázquez, A. V.; Chen, Z. Diffusion of One or More Components of a Silane Adhesion-Promoting Mixture into Poly(methyl methacrylate). *J. Colloid Interface Sci.* **2007**, *308*, 170−175.
(46) Vázquez, A. V.; Shephard, N. E.; Steinecker, C. L.; Ahn, D.; Spanninga, S.; Chen, Z. Understanding Molecular Structures of Silanes at Buried Polymer Interfaces Using Sum Frequency Generation Vibrational Spectroscopy and Relating Interfacial Structures to Polymer Adhesion. *J. Colloid Interface Sci.* **2009**, *331*, 408−416.
(47) Vázquez, A. V.; Boughton, A. P.; Shephard, N. E.; Rhodes, S. M.; Chen, Z. Molecular Structures of the Buried Interfaces between Silicone Elastomer and Silane Adhesion Promoters Probed by Sum Frequency Generation Vibrational Spectroscopy and Molecular Dynamics Simulations. *ACS Appl. Mater. Interfaces* **2010**, *2*, 96−103.
(48) Mark, A.; Chen, C.; Wang, J.; Chen, Z. Chemical Structures of Liquid Poly(ethylene glycol)s with Different End Groups at Buried Polymer Interfaces. *Macromolecules* **2006**, *39*, 9396−9401.
(49) Hirose, C.; Yamamoto, H.; Akamatsu, N.; Domen, K. Orientation Analysis by Simulation of Vibrational Sum Frequency Generation Spectrum: CH Stretching Bands of the Methyl Group. *J. Phys. Chem.* **1993**, *97*, 10064−10069.
(50) Bain, C. D. Sum-Frequency Vibrational Spectroscopy of the Solid/Liquid Interface. *J. Chem. Soc., Faraday Trans.* **1995**, *91*, 1281−1296.
(51) Baldelli, S.; Schnitzer, C.; Shultz, M. J.; Campbell, D. Sum Frequency Generation Investigation of Water at the Surface of H_2O/H_2SO_4 Binary Systems. *J. Phys. Chem. B* **1997**, *101*, 10435−10441.
(52) Morita, A.; Hynes, J. T. A Theoretical Analysis of the Sum Frequency Generation Spectrum of the Water Surface. II. Time-Dependent Approach. *J. Phys. Chem. B* **2002**, *106*, 673−685.
(53) Wang, C.; Groenzin, H.; Shultz, M. J. Surface Characterization of Nanoscale TiO_2 Film by Sum Frequency Generation Using Methanol as a Molecular Probe. *J. Phys. Chem. B* **2004**, *108*, 265−272.
(54) Zhang, C.; Wang, J.; Khmaladze, A.; Liu, Y.; Ding, B.; Jasensky, J.; Chen, Z. Examining Surface and Bulk Structures using Combined Nonlinear Vibrational Spectroscopies. *Opt. Lett.* **2011**, *36*, 2272−2274.
(55) Wang, J.; Mark, A.; Chen, X.; Schmaier, A. H.; Waite, J. H.; Chen, Z. Detection of Amide I Signals of Interfacial Proteins in Situ Using SFG. *J. Am. Chem. Soc.* **2003**, *125*, 9914−9915.
(56) Zheng, P.; McCarthy, T. J. Rediscovering Silicones: Molecularly Smooth, Low Surface Energy, Unfilled, UV/vis-Transparent, Extremely Cross-Linked, Thermally Stable, Hard, Elastic PDMS. *Langmuir* **2010**, *26*, 18585−18590.
(57) Kataoka, S.; Cremer, P. S. Probing Molecular Structure at Interfaces for Comparison with Bulk Solution Behaviro: Water/2-Propanol Mixtures Monitored by Vibrational Sum Frequency Spectroscopy. *J. Am. Chem. Soc.* **2006**, *128*, 5516−5522.
(58) Harp, G. P.; Rangwalla, H.; Yeganeh, M. S.; Dhinojwala, A. Infrared-Visible Sum Frequency Generation Spectroscopic Study of Molecular Orientation at Polystyrene/Comb-Polymer Interfaces. *J. Am. Chem. Soc.* **2003**, *125*, 11283−11290.
(59) Rao, A.; Rangwalla, H.; Varshney, V.; Dhinojwala, A. Structure of Poly(methyl methacrylate) Chains Adsorbed on Sapphire Probed

Using Infrared-Visible Sum Frequency Generation Spectroscopy. *Langmuir* **2004**, *20*, 7183−7188.
(60) Boughton, A. P.; Yang, P.; Tesmer, V. M.; Ding, B.; Tesmer, J. J. G.; Chen, Z. Heterotrimeric G Protein $\beta 1\gamma 2$ Subunits Change Orientation upon Complex Formation with G Protein-Coupled Receptor Kinase 2 (GRK2) on a Model Membrane. *Proc. Natl. Acad. Sci. U. S. A.* **2011**, *108*, E667−E673.
(61) Loch, C. L.; Ahn, D.; Chen, C.; Wang, J.; Chen, Z. Sum Frequency Generation Studies at Poly(ethylene terephthalate)/Silane Interfaces: Hydrogen Bond Formation and Molecular Conformation Determination. *Langmuir* **2004**, *20*, 5467−5473.